Geomechanics and Engineering, *Vol. 26, No. 3 (2021) 261-274*
https://doi.org/10.12989/gae.2021.26.3.261

End bearing capacity of embedded pile with inclined base plate: Field dynamic and static tests

Mi Jeong Seo[1a], Kyungsoo Han[2a], Jong-Bae Park[3b], Kyeong-Han Jeong[4b] and Jong-Sub Lee[*1]

[1]*School of Civil, Environmental and Architectural Engineering, Korea University, 145, Anam-ro, Seongbuk-gu, Seoul, 02841, Republic of Korea*
[2]*Lyles School of Civil Engineering, Purdue University, 550, Stadium Mall Drive, West Lafayette, Indiana, 47907, U.S.A.*
[3]*Land and Housing Institute, Korea Land & Housing Corporation, 99, Expo-ro 539beon-gil, Yuseong-gu, Daejeon, 34047, Republic of Korea*
[4]*The Dream ENC, 361, Simin-daero, Dongan-gu, Anyang-si, Gyeonggi-do, 14057, Republic of Korea*

(Received December 2, 2020, Revised July 30, 2021, Accepted August 2, 2021)

Abstract. The objective of this study is to investigate the effects of incorporating inclined base plates on the end bearing capacities of embedded piles by conducting dynamic pile tests and static load tests. Two types of embedded piles were prepared – conventional piles with a 50-cm-diameter flat base plate and piles with a 56-cm-diameter inclined base plate. The dynamic pile tests were conducted during pile construction, and the static load tests were conducted after curing the cement paste to investigate the end bearing capacities of the test piles. Test results indicate that the base resistances of piles with inclined base plates are greater than those of conventional piles and that the base resistances increase with an increase in the inclination angle. The increased projected area, increased contact area, extended rupture surface, and enhanced slime discharge due to the inclined base plate may result in an increase in the end bearing capacity of the pile. This study demonstrates that the end bearing capacities of the embedded piles may be maximized by incorporating inclined plates to the pile base. Thus, the pile with the inclined base plate may be effectively used for the construction of embedded piles.

Keywords: dynamic pile test (DPT); embedded pile; end bearing capacity; inclined base plate; static load test (SLT)

1. Introduction

Pile foundations may be categorized according to their construction methods into two types, which are displacement piles and non-displacement piles. A driven pile is generally categorized as a displacement pile, whereas embedded piles and bored piles are typical non-displacement piles (Karkee 1999). Notably, the use of driven piles causes problems such as high noise and large vibrations generated during construction. Consequently, embedded piles and bored piles are commonly used to reduce noise and vibrations (Hong and Chai 2003, Hong *et al*. 1997, Karkee 1999, Zou *et al*. 2019). Embedded piles are precast piles inserted into the ground with cement paste after boring, whereas bored piles are formed by concreting with reinforcement steel. In Japan, environmental pollution due to construction sites became an issue after noise and vibration control acts were introduced in 1968 and 1976, respectively. Thus, the embedded pile method was developed to minimize the noise and vibration levels generated during pile installation, and the application of embedded piles has rapidly spread in Japan (Karkee 1999). Similarly, noise and vibration control acts introduced in Korea in 1994 led to a surge in the use of embedded piles in Korea. Presently, driven piles are rarely used in Korea except in offshore projects.

The construction process of the embedded pile, which is commonly employed in Korea, is illustrated in Fig. 1. The process begins with boring the ground to a desired depth as shown in Figs. 1(a) and 1(b). To obtain sufficient bearing capacity, boring is conducted until the borehole reaches a stiff layer, such as weathered rock as shown in Fig. 1(b). A screw-shaped auger, whose diameter exceeds that of the pile by 10 cm, is employed (Hong *et al*. 1997) in combination with an outer casing to prevent the collapse of the hole. The outer casing and inner auger rotate in opposite directions to excavate the ground (Hong and Chai 2003, Hong *et al*. 1997). After the excavation is completed, the inner auger is extracted (Fig. 1(c)), and a precast pile is inserted into the borehole, while the outer casing remains in the ground (Fig. 1(d)). Precast concrete piles and steel pipe piles are commonly employed as embedded piles. When the pile base arrives at the end of the borehole, cement paste is injected, and the outer casing is pulled out (Fig. 1(e)). The final tapping is performed using a drop hammer to fix the pile base into the soil as shown in Fig. 1(f) (Hong *et al*. 1997, Karkee 1999, Hong and Chai 2003).

The bearing capacity of a pile foundation is equal to the sum of the end bearing capacity and the skin friction. An embedded pile contains a gap between the borehole and

*Corresponding author, Professor, Ph.D.
E-mail: jongsub@korea.ac.kr
[a]Ph.D. Student
[b]Ph.D.

ISSN: 2005-307X (Print), 2092-6219 (Online)

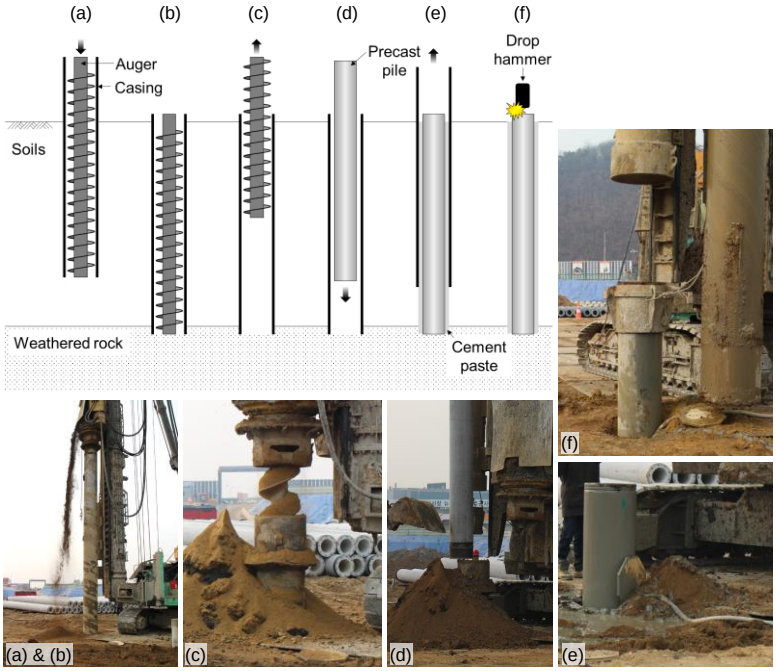

Fig. 1 Embedded pile construction process: (a) boring with inner auger and outer casing, (b) reaching weathered rocks, (c) pulling out inner auger, (d) inserting precast pile, (e) injecting cement paste and pulling out outer casing and (f) tapping with a drop hammer

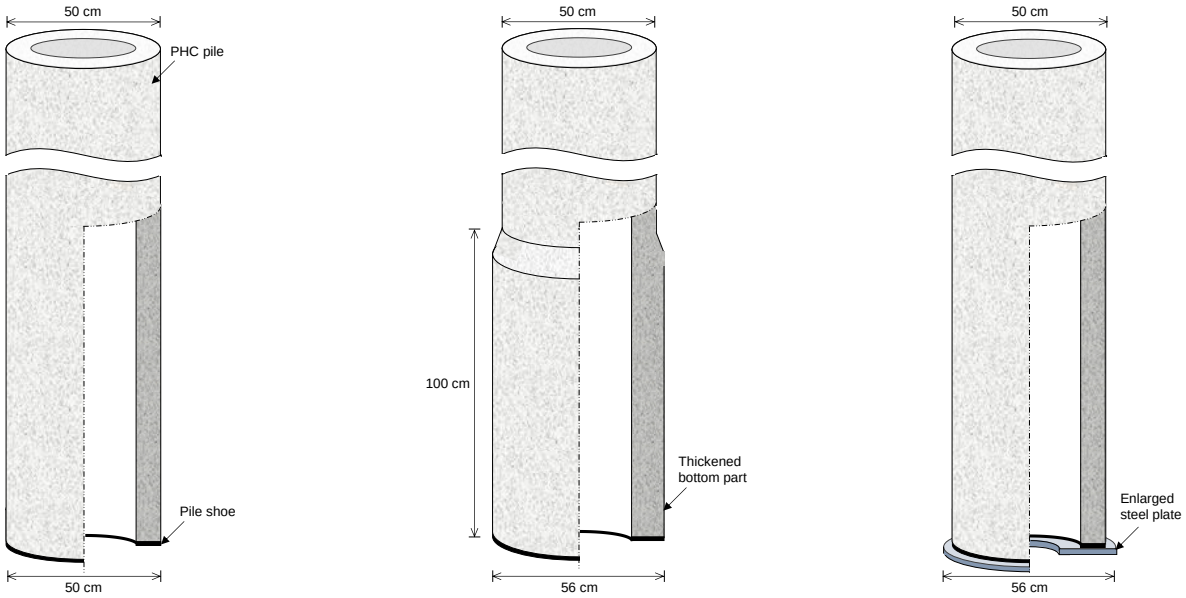

(a) Conventional pile (b) Pile with thickened bottom part (c) Pile with enlarged steel plate

Fig. 2 Conceptual diagrams for different base shapes of embedded piles

pile. Thus, cement paste should be injected into the space and cured to obtain sufficient skin friction. However, the cement paste could be washed away due to groundwater flow through loosened soils, leading to insufficient skin friction. Thus, the end bearing capacity of an embedded pile should be sufficient to support the superstructure. A common method of enhancing the end bearing capacity of an embedded pile involves enlargement of the pile base as shown in Fig. 2. A conventional concrete pile is illustrated in Fig. 2(a) for comparison. Fig. 2(b) shows a pile, of which the base area is enlarged by thickening the bottom part of the pile. Lastly, Fig. 2(c) shows a pile with an enlarged steel plate attached to its base. The pile illustrated in Fig. 2(c) is commonly used in Korea, and extensive model tests, field tests, and numerical studies have been conducted based on this method (Yoo *et al*. 2007). The end bearing capacities of the enlarged piles, illustrated in Figs. 2(b) and 2(c), may be higher than that of the conventional pile shown in Fig. 2(a) because of the larger base areas.

In this study, the effects of the inclined base plate on the

Table 1 Dimensions of base plate

Pile type	Base plate diameter [cm]	Inclination angle, α [°]	Height, h [cm]	Projected area, A_p [cm^2]	Contact area, A_c [cm^2]
Pile-C	50	-	-	1963.5	1963.5
Pile-I30	56	30	4.0	2463.0	2529.6
Pile-I45	56	45	5.5	2463.0	2664.3
Pile-I60	56	60	8.5	2463.0	3009.9

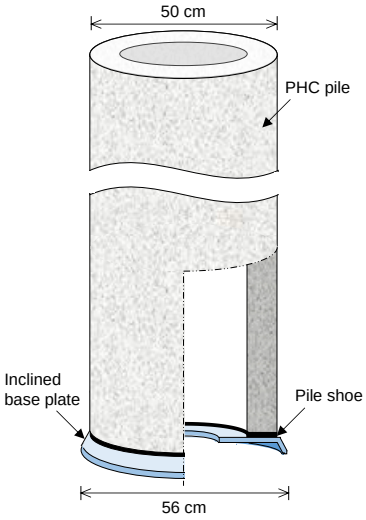

(a) Three-dimensional diagram

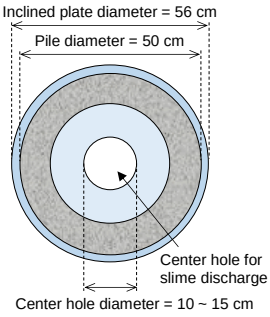

(b) Top view diagram

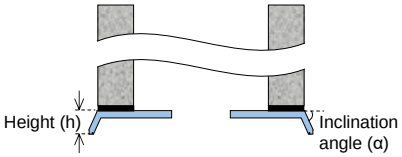

(c) Side view diagram

(c) Attached by welding

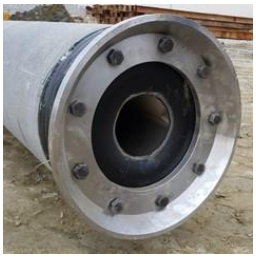

(d) Attached by bolting

Fig. 3 Pile with inclined base plate

end bearing capacity of embedded piles were investigated by performing dynamic pile tests and static load tests in the field. The inclined base plates were attached to the bases of piles. Test piles with diameters of 50 cm were installed in two fields and divided into four types: a conventional pile (Pile-C) and piles with base plates inclined at 30°, 45°, and 60° with diameters of 56 cm (Pile-I30, I45, and I60, respectively). The base resistances of the piles were evaluated by performing dynamic pile tests during pile construction. Static load tests were conducted after curing of the cement paste to determine the base resistances of piles according to the inclination angle of the base plates. Finally, the increase in the end bearing capacity of the pile is analyzed quantitatively in terms of the increased projected area, increased contact area, and extended rupture surface, and discussed qualitatively based on the enhanced slime discharge.

2. Experimental setup

2.1 Test piles

Test piles were installed at two test sites (Sites A and B), and load tests were conducted to investigate the base resistances of the piles according to the base shape. Three-dimensional, top, and side views of piles with inclined base plates are presented in Figs. 3(a), 3(b), and 3(c), respectively. Test piles are pretensioned high spun concrete (PHC) piles with a diameter of 50 cm and thickness of 8 cm. The diameter of the inclined base plate is 56 cm, exceeding the pile diameter by 6 cm. Thus, in this study, an inclined base plate refers to the inclined enlarged base plate. Note that the conventional pile with the flat base plate and the piles with the inclined enlarger base plates are named Pile-C and Pile-Is, respectively. Particularly, the piles with the base plates inclined at 30°, 45°, and 60° are named Pile-I30, Pile-I45, and Pile-I60, respectively. Dimensions of Pile-C and Pile-Is are summarized in Table 1. The shape of the pile base is described by the inclination angle (α) as depicted in Fig. 3(c). The thickness of all the inclined base plates is 2.5 cm. As α increases, the inclined part of the base plate lengthens downwards. Thus, the heights (h) of the inclined base plates for Pile-I30, Pile-I45, and Pile-I60 are 4.0, 5.5, and 8.5 cm, respectively, as summarized in Table 1. The projected and contact areas of the test piles are

Table 2 Summary of test piles and field test conditions

	Site	Site A	Site B
Pile	Pile diameter	50 cm	50 cm
	Borehole diameter	60 cm	60 cm
	Pile length	12 m	14 m
	Pile base shape	Conventional pile: Pile-C Pile with 30° inclined base plate: Pile-I30 Pile with 45° inclined base plate: Pile-I45 Pile with 60° inclined base plate: Pile-I60	Conventional pile: Pile-C Pile with 45° inclined base plate: Pile-I45 Pile with 60° inclined base plate: Pile-I60
Plate	Base plate diameter	Conventional pile: 50 cm Pile with inclined base plate: 56cm	Conventional pile: 50 cm Pile with inclined base plate: 56cm
	Center hole diameter	10 cm	15 cm
	Attached method	Welding	Bolting
Ground	SPT N-value near pile base	50/6–50/2	50/8–50/4
Test	Type of experiments	Dynamic pile test	Dynamic pile test, Static load test

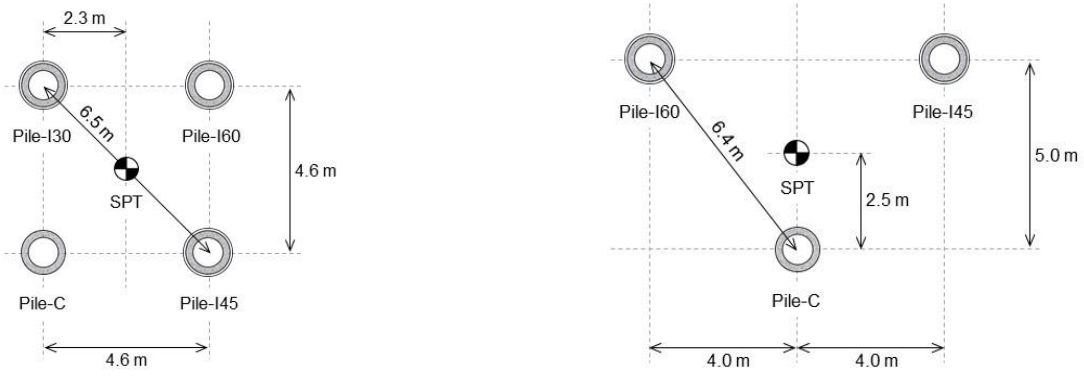

(a) Site A (b) Site B

Fig. 4 Test pile arrangement

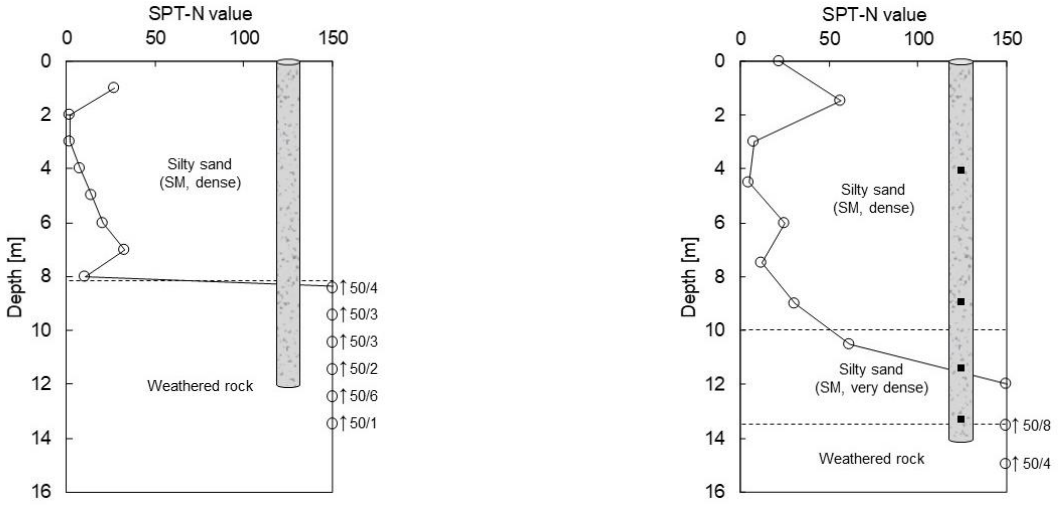

(a) Site A (b) Site B

Fig. 5 SPT N-values with respect to depth (The circles with arrows (○↑) indicate SPT N-values above 150/30, and the solid squares (■) denote the locations of vibrating wire type strain gauges)

summarized in Table 1. Note that the projected area (A_p) is defined as the closed-ended cross-sectional area of the pile base, which corresponds to the total area of the top view diagram as shown in Fig. 3(b). The projected areas of Pile-C and Pile-Is are 1963.5 and 2463.0 cm^2, respectively. In addition, the contact area (A_c) is the area of the pile base touched by the soils. The contact area of Pile-C is the same as the projected area because the base of Pile-C is flat. Meanwhile, the contact areas of Pile-Is are the summation of the area of the flat part and that of the inclined part. For Pile-Is, the contact area increases from 2529.6 to 3009.9 cm^2 as the inclination angle increases from 30 to 60°, as

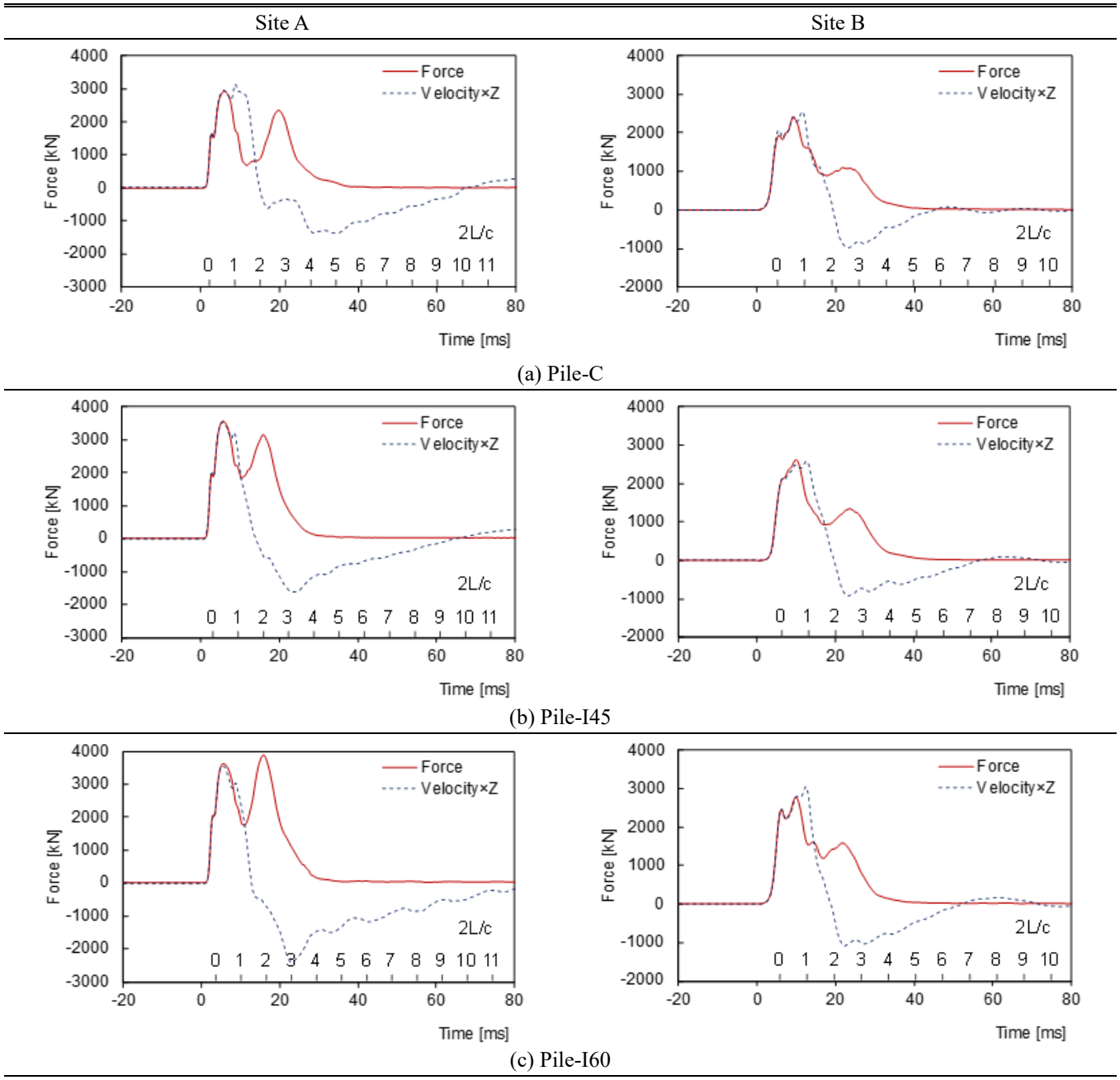

Fig. 6 Measured force and velocity signals at pile heads at Sites A and B (Z denotes the impedance of the pile)

summarized in Table 1.

The pile installation and load tests are detailed in Table 2. The borehole diameters of Sites A and B are same as 60 cm. A hole was made at the center of the base plate to discharge the slime produced below the pile base. The diameters of the center holes at Sites A and B are 10 cm and 15 cm, respectively, whereas the corresponding pile lengths are 12 m and 14 m, respectively. The inclined base plate was attached to the pile base by welding (at Site A) or bolting (at Site B) as shown in Figs. 3(d) and 3(e), respectively.

2.2 Test setup

The test pile arrangements at Sites A and B are presented in Figs. 4(a) and 4(b), respectively. Fig. 4 shows that Pile-C, I30, I45, and I60 were installed at Site A, whereas only Pile-C, I45, and I60 were installed at Site B. The shortest distance between the piles is 4.6 m at Site A and 6.4 m at Site B. Standard Penetration Tests (SPTs) were performed to investigate the ground conditions. SPTs were performed at the midpoints of the test piles at both sites, as shown in Figs. 4(a) and 4(b). The obtained SPT N-values with respect to depth are plotted in Fig. 5. The soils near the upper part of the piles at Sites A and B are classified as silty sands (SM) using the unified soil classification system. In contrast, the ground near the pile bases is weathered rock, of which the SPT N-values are 50/6–50/2 and 50/8–50/4 at Sites A and B, respectively. The end bearing capacities of the piles installed at Site A may be higher than those

installed at Site B, as the penetration depth of piles into the weathered rock at Site A is greater than that at Site B. Accordingly, the SPT N-values near the pile base are larger at Site A than Site B.

The test piles at Sites A and B were installed using the embedded pile method as described in Fig. 1. At Site A, the piles were tapped by drop hammers with a ram weight of 60 kN at a drop height of 2.0 m. The ram weight and drop height of the hammer employed at Site B were 50 kN and 1.5 m, respectively. The base resistances of the piles in terms of the base shapes were evaluated by load tests. First, dynamic pile tests (DPTs) were performed during pile construction at Sites A and B according to ASTM D4945, to investigate the base resistance prior to curing of the cement paste. After curing was completed, static load tests (SLTs) were performed at Site B. SLTs were performed using quick methods according to ASTM D1143, wherein loads were applied to pile heads using reaction anchors and hydraulic jacks. The resistance and settlement were measured at pile heads using a loadcell and linear variable differential transformers. Vibrating wire type strain gauges were preinstalled on tendons during the fabrication of precast piles for the evaluation of resistance and settlement at pile bases, as shown in Fig. 5(b). Four pairs of strain gauges were located at 0.5, 2.5, 5.0, and 10.0 m from the pile toe. The transferred loads at each load step are estimated from measured strains by multiplying the elastic modulus and cross-sectional area of the pile. The base resistance is obtained by extrapolating from the estimated transferred loads at locations 0.5 m and 2.5 m from the pile toe. Meanwhile, elastic shortening along the pile can be estimated by the transferred load, length, and stiffness of the pile segment, which can be calculated using the elastic modulus and cross-sectional area of the pile (Fellenius 2002, Fellenius *et al*. 2009, Fellenius and Terceros 2014). Finally, the base settlement at each load step is calculated by subtracting the elastic shortening along the pile from the head settlement. Note that a telltale cannot be instrumented as the thickness of the test pile is only 80 mm, which is not sufficient to install a telltale pipe.

3. Experimental results

3.1 Dynamic pile tests (Site A)

Test piles were tapped to collect the force and velocity waveforms, which were measured by a couple of strain gauges and accelerometers installed on both sides of the test piles approximately 1 m below the pile heads. Field data were acquired and processed using the pile driving analyzer. A drop hammer with a ram weight of 60 kN was employed in the DPTs at Site A, where the test piles were tapped three times at the drop height of 2.0 m. The energy transferred to pile heads by drop hammer tapping is in the range of 55–77 kJ. The force and velocity waveforms measured during DPTs performed at Site A are plotted in Fig. 6. Figs. 6(a), 6(b), and 6(c) present the results obtained for Pile-C, I45,and I60, respectively. Note that the waveforms of Pile-I30 are similar to those of Pile-C. Load – settlement curves determined from the force and velocity waveforms are plotted using CAse Pile Wave Analysis Program (CAPWAP) in Fig. 7. Figs. 7(a) and 7(b) present load – settlement curves of piles with different base shapes at the pile head and base, respectively. The elastic modulus and wave speed, used as inputs in CAPWAP analyses at Site A, are 35,000 MPa and 3,800 m/s, respectively. The toe quakes range from 15 to 20 mm and the toe damping factors are about 0.22 s/m at Site A. The toe quakes for embedded piles are generally large compared to those for the driven piles (~5 mm) in very dense or hard soils due to the slime, which is loosened soils combined with water near the pile base during the excavation of boreholes (Pile Dynamics Inc. 2014). The toe damping factor (0.22 s/m) at Site A is slightly below the recommended value of 0.25 s/m, because the base was placed on compacted slime and the weathered rock. The head resistances of all Pile-Is (Pile-I30, I45, and I60) are larger than that of Pile-C for all head settlements, as shown in Fig. 7(a). Furthermore, head resistances increase with an increase in the inclination angle (α). Fig. 7(b) indicates that base resistances of Pile-Is are also higher than that of Pile-C and increase with an increase in the inclination angle.

The base resistances (Q_b) of piles with different base shapes, estimated from the load – settlement curves (Fig. 7) at the base settlement of 15 mm (s = 15 mm) and the maximum base settlement (max. s), are summarized in Table 3. Q_b of Pile-C evaluated at s = 15 mm is 1543 kN, whereas those of Pile-I30, I45, and I60 are 2358, 2915, and 3499 kN, respectively. For comparison, Q_b increments of Pile-Is are likewise summarized in Table 3. Note that the Q_b increment is defined as the ratio of Q_b of Pile-Is to Q_b of Pile-C. Thus, the Q_b increments at s = 15 mm for Pile-I30, I45, and I60 are observed to be 52.8%, 89.0% and 126.8%, respectively. Q_b of Pile-Is at s = 15 mm is observed to be significantly larger than that of Pile-C, as reflected in the large differences between the initial slopes of the respective load – settlement curves. Fig. 7(b) shows that the load – settlement curves of Pile-Is are relatively stiff compared to those of Pile-C for all settlements. Meanwhile, Q_b of Pile-C estimated at max. s is 2120 kN, whereas Q_b of Pile-I30, I45, and I60 are 2894, 3152, and 3834 kN, respectively. Fig. 7(b) shows that Q_b of all test piles reach the ultimate values. The Q_b increments obtained at max. s are also summarized in Table 3 for comparison. The Q_b increments of Pile-I30, I45, and I60 at max. s are observed to be 36.5%, 48.7%, and 80.8%, respectively. The Q_b increments of Pile-Is obtained at max. s are relatively small compared to those obtained at s = 15 mm.

3.2 Dynamic pile tests (Site B)

The ram weight and drop height of the drop hammer used at Site B were 50 kN and 1.5 m, respectively. The test piles at Site B were tapped three times for the DPTs. The energy transferred to pile heads at Site B by hammer tapping is in the range of 42–55 kJ. The force and velocity waveforms measured during DPTs are plotted in Fig. 6. Figs. 6(a), 6(b), and 6(c) represent the waveforms obtained from Pile-C, I45, and I60, respectively. The elastic modulus and wave speed of the piles at Site B are 39,000 MPa and 4,000 m/s, respectively, which are slightly higher than those

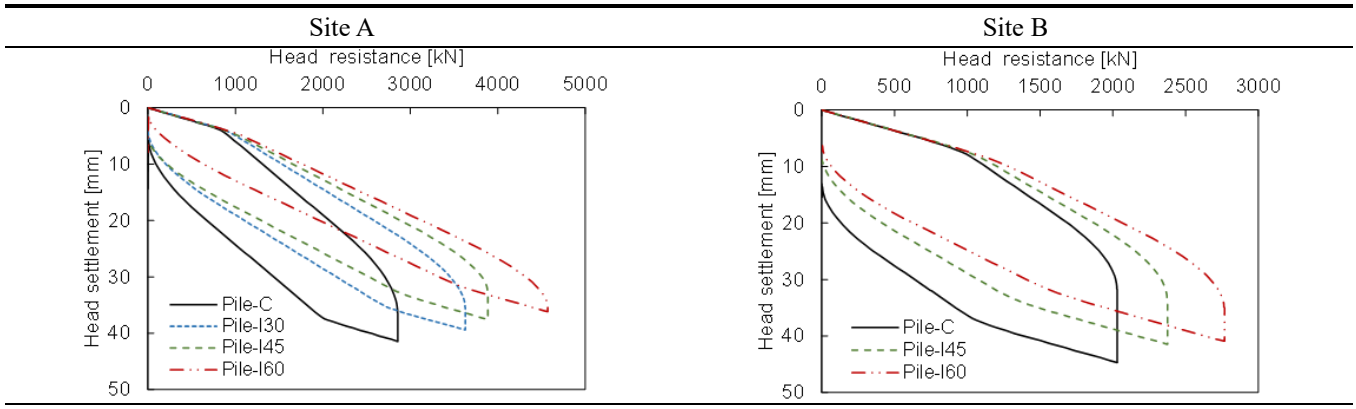

(a) Head resistance verses head settlement

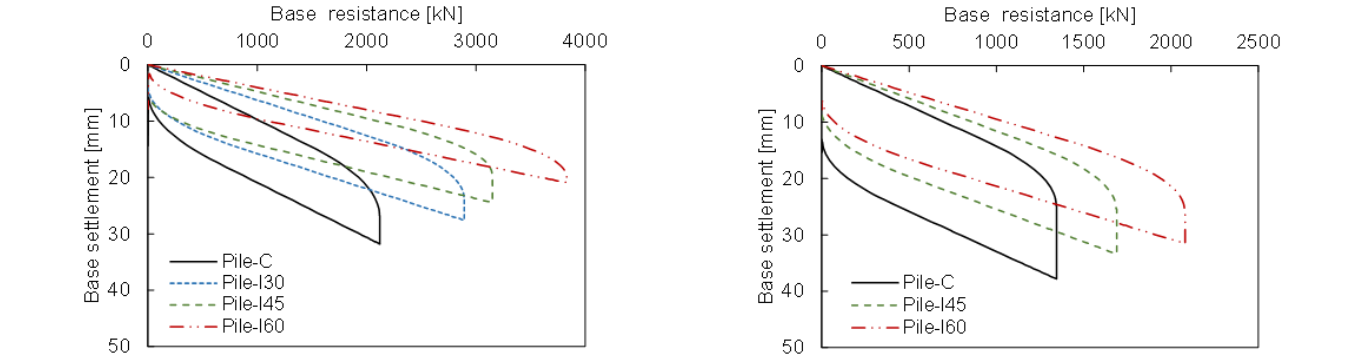

(b) Base resistance versus base settlement

Fig. 7 Load-settlement curves obtained by dynamic pile tests at Sites A and B

Table 3 Base resistance (Q_b) according to pile base shape

Pile type	Dynamic pile test								Static load test						Average increment of Q_b at max. s or s = 40 mm [%]*	Lab test (Han *et al.* 2020)**	
	Site A				Site B				Site B							s = 10% of pile diameter	
	s = 15 mm		max. s		s = 15 mm		max. s		s = 10 mm		s = 15 mm		s = 40 mm				
	Q_b [kN]	Increment [%]	Q_b [kN]	Increment [%]	Q_b [kN]	Increment [%]	Q_b [kN]	Increment [%]	Q_b [kN]	Increment [%]	Q_b [kN]	Increment [%]	Q_b [kN]	Increment [%]		Q_b [kN]	Increment [%]
Pile-C	1543	-	2120	-	1046	-	1344	-	1190	-	1508	-	1894	-	-	1.68	-
Pile-I30	2358	52.8	2894	36.5	-	-	-	-	-	-	-	-	-	-	36.5	2.14	27.5
Pile-I45	2915	89.0	3152	48.7	1285	22.8	1689	25.7	1283	7.8	1712	13.5	3355	77.2	50.5	2.42	44.1
Pile-I60	3499	126.8	3834	80.8	1578	50.8	2081	54.8	1943	63.3	2665	76.7	-	-	67.8	2.87	70.8

· s denotes the base settlement.
· The increment is the ratio of Q_b of Pile-Is to Q_b of Pile-C.
* Average Q_b increment is calculated using Q_b at max. s or s = 40 mm by the field tests at Sites A and B.
** Q_b is evaluated at the fixed vertical stress of 100 kPa.

at Site A. This is because, the piles at Site A are manufactured using a non-autoclave process, whereas those at Site B are manufactured employing an autoclave process. Note that piles manufactured using an autoclave process are generally stiffer than those produced without an autoclave process. The toe quakes used in CAPWAP analyses at Site B are 19–20 mm, which are slightly higher than those at Site A, because the SPT N-value near the pile base is larger at Site A than Site B. The toe damping factors at Site B are about 0.25 s/m, which are almost the same as at Site A. The shapes of the waveforms measured at Site B are similar to those at Site A. However, the forces measured by the strain gauge and the velocities at Site B are smaller than those at Site A because of the lower tapping energy. The load – settlement curves obtained for pile heads and bases using CAPWAP are plotted in Figs. 7(a) and 7(b), respectively. Fig. 7 shows that the head and base resistances of Pile-Is are greater than those of Pile-C for all settlements. The head and base resistances increase with an increase in the inclination angle (α) of the base plate.

Q_b of Site B estimated at the base settlement of 15 mm (s = 15 mm) and maximum settlement (max. s) in Fig. 7(b)

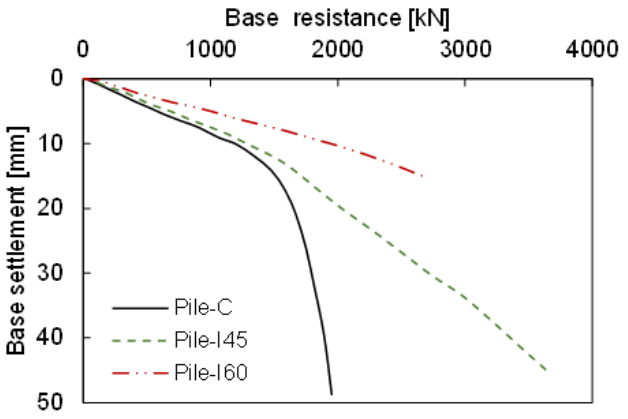

Fig. 8 Load-settlement curves at pile bases obtained by static load tests at Site B

for piles with different base shapes are summarized in Table 3. Q_b at s = 15 mm of Pile-C, I45, and I60 are 1046, 1285, and 1578 kN, respectively, and the Q_b increments at s = 15 mm of Pile-I45 and I60 compared with Pile-C are 22.8% and 50.8%, respectively. Furthermore, Q_b at max. s of Pile-C is 1344kN, whereas those of Pile-I45 and I60 are 1689 kN and 2081 kN, respectively. The corresponding Q_b increments at max. s of Pile-I45 and I60 compared with Pile-C are 25.7% and 54.8%, respectively. Table 3 indicates that the Q_b increments obtained at max. s are almost identical to those obtained at s = 15 mm. For the same base shape, Q_b observed at Site B is smaller than that observed at Site A, as the SPT N-values at Site B (50/8–50/4) are smaller than those at Site A (50/6–50/2), and the transferred energies at Site B (42–55 kJ) are smaller than those at Site A (55–77 kJ).

3.3 Static load tests (Site B)

The load – settlement curves at pile bases estimated by SLTs are plotted in Fig. 8. Fig. 8 shows that the load – settlement curves of Pile-Is are stiffer than those of Pile-C. Furthermore, the base resistance increases with an increase in the inclination angle (α) for all base settlements. The base resistances (Q_b) at base settlements of s = 10, 15, and 40 mm and the Q_b increments are summarized in Table 3. Q_b at a base settlement of 10 mm (s = 10 mm) of Pile-C, I45, and I60 are 1190, 1283, and 1943 kN, respectively. Thus, the Q_b increments of Pile-I45 and I60 are 7.8% and 63.3%, respectively. For a base settlement of 15 mm (s = 15 mm), Q_b of Pile-C is 1508 kN, whereas Q_b of Pile-I45 and I60 are 1712 kN and 2665 kN, respectively, which indicate increments of 13.5% and 76.7%, respectively, compared to Q_b of Pile-C. Lastly, at a base settlement of 40 mm (s = 40 mm), Q_b of Pile-C and I45 are 1894 kN and 3355 kN, respectively. Q_b of Pile-I60 at a base settlement of 40 mm is not estimated, as the base settlement of Pile-I60 does not reach 40 mm.

The Q_b increment of Pile-I45 at a base settlement of 40 mm is 77.2%, whereas that at a base settlement of 10 mm is 7.8%. Fig. 8 shows that the load – settlement curve of Pile-I45 is similar to that of Pile-C when the base resistances are below 1200 kN. For Pile-C, the base settlement increases significantly when the base resistance exceeds 1700 kN, whereas the base settlement of Pile-I45 exhibits a gradual increase. The base resistance of Pile-C becomes 2000 kN, which may be the ultimate capacity for base settlements exceeding 30 mm. In contrast, no ultimate capacity is observed for Pile-I45. However, for Pile-I45, the stiffness of the load – settlement curve is slightly reduced after the base resistance reaches 1800 kN, exhibiting bilinear behavior. The load – settlement curve of Pile-I45 remains linear even until the base resistance reaches the maximum test load of 3700 kN at the pile base. Furthermore, the base settlement of Pile-I60 is significantly smaller than that of Pile-I45 or Pile-C.

4. Analyses and discussion

The base resistances (Q_b) and the corresponding Q_b increments relative to the conventional pile (Pile-C) are summarized in Table 3, respectively. Note that Q_b and the Q_b increments are estimated from the base resistances at base settlements of 15 mm (s = 15 mm) and 40 mm (s = 40 mm), and maximum base settlement (max. s). At the same base settlement, the base resistances obtained at Site A are greater than those at Site B, because the SPT N-values of Site A are greater than those of Site B. In addition to the results of the field tests conducted in this study, those of the laboratory tests conducted by Han *et al.* (2020) are summarized in Table 3. Han *et al.* (2020) conducted laboratory tests on piles with inclined base plates, which are reduced to a length scale of one-tenth of the real size. Table 3 show that Q_b of Pile-Is are higher compared to those of Pile-C, and that Q_b generally increases with an increase in the inclination angle (α). As a result of the field tests, the Q_b increments of piles with base plates inclined at 30°, 45°, and 60° (Pile-I30, I45 and I60, respectively) are in the ranges of 36.5–52.8%, 7.8–89.0%, and 50.8–126.8%, respectively. The average Q_b increments of Pile-I30, I45, and I60 at the relatively large base settlement (max. s or s = 40 mm) are 36.5, 50.5, and 67.8%, respectively, as summarized in Table 3. On the other hand, for the laboratory tests, the Q_b increments of Pile-I30, I45, and I60 are evaluated as 27.5, 44.1, and 70.8%, respectively (see details in Han *et al.* (2020)). Note that the Q_b obtained from the laboratory tests are the base resistances at the base settlement of s = 10% of the pile diameter at the fixed vertical stress of 100 kPa. The Q_b increments of the piles with different base shapes are analyzed quantitatively and qualitatively according to the inclination angle. The projected area and contact area of pile bases, both of which increase upon the incorporation of the inclined base plate, are considered first. Note that the projected area is defined as the closed-ended cross-sectional area of the whole pile base. Subsequently, changes in the rupture surface are analyzed in terms of the inclination angle (α). Lastly, the effect on slime discharge upon the incorporation of the inclined base plate is discussed.

4.1 Quantitative factors

4.1.1 Increased projected area

The higher Q_b of Pile-Is than those of Pile-C may result

Table 4 Projected area, contact area, and rupture surface according to pile base shape

Pile type	Projected area		Contact area		Rupture surface calculation					
					Inclination angel, α [°]	Experimental parameter, β [°]	Bearing capacity factor		Rupture surface	
	A_p [cm^2]	Increment [%]	A_c [cm^2]	Increment [%]			N_q^* []	Increment [%]	S_r ($A_p \times N_q^*$) [cm^2]	Increment [%]
Pile-C	1963.5	-	1963.5	-	0	0	64.20	-	126,047	-
Pile-I30	2463.0	25.4	2529.6	28.8	30	0.5	73.90	15.1	182,009	44.4
Pile-I45	2463.0	25.4	2664.3	35.7	45	0.75	79.39	23.7	195,541	55.1
Pile-I60	2463.0	25.4	3009.9	53.3	60	1	85.37	33.0	210,276	66.8

· The increment is the ratio of A_p, A_c, N_q^*, and S_r of Pile-Is to those of Pile-C.
· For the calculation of the rupture surfaces, the effective stresses of all piles are assumed to be the same.
· N_q^* is calculated assuming that the friction angle of the soils is 40°.

Table 5 Unit base resistance (q_b) according to pile base shape

Pile type	Dynamic pile test								Static load test				Average increment of q_b at max. s or s = 40 mm [%]*	Lab test (Han *et al.* 2020)**	
	Site A				Site B				Site B					s = 10% of pile diameter	
	s = 15 mm		max. s		s = 15 mm		max. s		s = 15 mm		s = 40 mm				
	q_b [MPa]	Increment [%]	q_b [MPa]	Increment [%]	q_b [MPa]	Increment [%]	q_b [MPa]	Increment [%]	q_b [MPa]	Increment [%]	q_b [MPa]	Increment [%]		q_b [MPa]	Increment [%]
Pile-C	7.86	-	10.80	-	5.33	-	6.84	-	7.68	-	9.65	-	-	0.86	-
Pile-I30	9.57	21.9	11.75	8.8	-	-	-	-	-	-	-	-	8.8	0.87	1.6
Pile-I45	11.84	50.7	12.80	18.5	5.22	-2.1	6.86	0.2	6.95	-9.5	13.62	41.2	20.0	0.98	14.9
Pile-I60	14.20	80.8	15.57	44.2	6.41	20.3	8.45	23.4	10.82	40.9	-	-	33.8	1.17	36.2

· s denotes the base settlement.
· The increment is the ratio of q_b of Pile-Is to q_b of Pile-C.
* Average q_b increment is calculated using q_b at max. s or s = 40 mm by the field tests at Sites A and B.
** q_b is evaluated at the fixed vertical stress of 100 kPa.

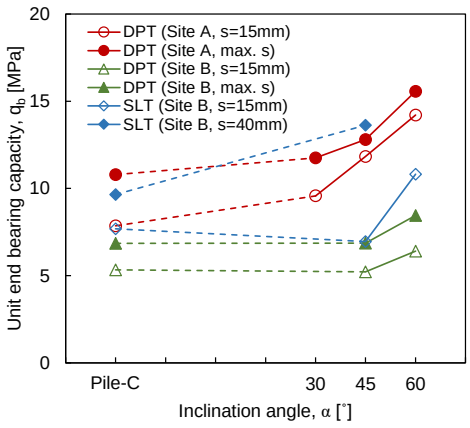

(a) Unit base resistance

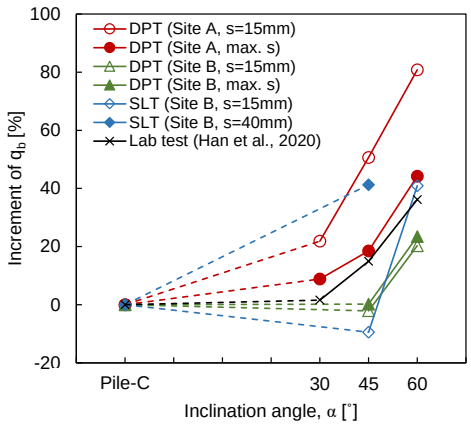

(b) Increments of unit base resistance in pile with inclined base plate compared to conventional pile

Fig. 9 Unit base resistance according to pile base shape (Note that q_b obtained by the laboratory test refers to the base resistance at the base settlement of 10% of the pile diameter)

from the larger projected area (A_p), as the base diameter of Pile-Is exceeds that of Pile-C. All test piles used in this study are PHC piles with diameters of 50 cm, and A_p of Pile-C is 1963.5 cm^2 as summarized in Table 4. In contrast, A_p of Pile-Is is 2463.0 cm^2, which is 25.4% larger than that of Pile-C, resulting from the larger diameter of the inclined base plate at 56 cm. To eliminate the effect of the increased A_p, the unit base resistance (q_b) for each test pile is obtained by normalizing to the area of the base plate, as summarized in Table 5. For the field test results, q_b of Pile-C is obtained by dividing Q_b by 1963.5 cm^2, whereas those of Pile-Is are obtained by dividing Q_b by 2463.0 cm^2. On the other hand, q_b of Pile-C and Pile-Is for the laboratory tests are obtained

by dividing Q_b by 19.64 and 24.63 cm^2, respectively. q_b and the q_b increments are plotted with respect to the pile base shape, as represented in Figs. 9(a) and 9(b). Note that the q_b increments of Pile-Is correspond to the ratios of q_b of Pile-Is and Pile-C. The results of the DPTs indicate that q_b of Pile-Is typically exceed those of Pile-C, and q_b increases with an increase in α as shown in Fig. 9(b). q_b of Pile-I30, which is only installed at Site A, exhibits an 8.8–21.9% increase compared to that of Pile-C as summarized in Table 5. q_b of Pile-I45 are observed to increase by 18.5–50.7% compared to those of Pile-C at Site A, whereas at Site B, q_b of Pile-I45 and Pile-C are almost identical. q_b of Pile-I60 exhibits an increase of 20.3–80.8% compared to that of Pile-C. For the SLTs performed at Site B, q_b of Pile-I45 at a base settlement of 15 mm is smaller than q_b of Pile-C, because of the small base settlement, as summarized in Table 5. However, q_b of Pile-I45 corresponding to a relatively large base settlement of 40 mm exhibits an increase of 41.2%, compared to that of Pile-C. Furthermore, q_b of Pile-I60, which corresponds to the base resistance at a base settlement of 15 mm, exceeds that of Pile-C by 40.9%. In addition, the average q_b increments at the relatively large base settlement (max. s or s = 40 mm) are summarized in Table 5. The average q_b increments at the relatively large base settlements are 8.8, 20.0, and 33.8% for Pile-I30, I45, and I60, respectively. Table 5 and Fig. 9 suggest that the inclined base plate may have additional effects on Q_b, as q_b increases with an increase in the inclination angle (α), although A_p remains the same for all Pile-Is.

4.1.2 Increased contact area

The base area of a pile foundation typically indicates the projected area of the pile base. The contact area (A_c) between the pile base and soils likewise affects Q_b (Huat *et al*. 2007, Mohamed and Austrell 2018). A_p of all Pile-Is are identical and, typically, exceed that of Pile-C by 25.4% as summarized in Table 4. However, A_c increases with anincrease in the inclination angle (α), as the inclined part of the base plate becomes longer, although the base diameters of all Pile-Is are fixed at 56 cm. For a quantitative comparison of areas, A_c for all piles are calculated as summarized in Table 4. Both A_c and A_p of Pile-C are 1963.5 cm^2, because of the flat base. Meanwhile, A_c of Pile-Is exceed that of the corresponding A_p (2463.0 cm^2). The increments in A_c with respect to the increase in the inclination angle are summarized in Table 4. For Pile-I30, the A_c increment is 28.8%, which is similar to the A_p increment of 25.4%. Correspondingly, the A_c increments of Pile-I45 and I60 are 35.7% and 53.3%, respectively, exceeding the A_p increment of 25.4%. Table 4 indicates that the A_c increments increase with an increase in the inclination angle. The experimental results summarized in Table 3, likewise indicate that the Q_b increments of Pile-I30 are relatively small compared to those of Pile-I45 and I60. The observed trend concerning the A_c increment may be one of the factors contributing to this tendency.

The Q_b increments are plotted against the A_c increments in Fig. 10, which shows that the Q_b increments increase with an increase in the A_c increment. The effects of the

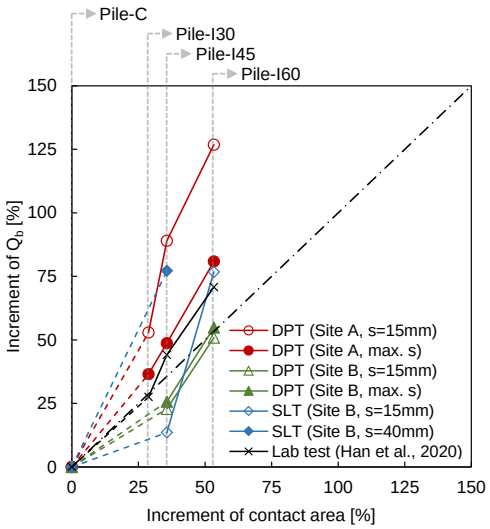

Fig. 10 Increment of contact area versus increment of base resistance (Note that Q_b obtained by the laboratory test refers to the base resistance at the base settlement of 10% of the pile diameter)

inclined base plates on Q_b may be explained with reference to the concept of the shell foundation. A shell foundation, the shape of which is similar to the base of Pile-Is, exhibits a higher bearing capacity at larger inclination angles (α), because of the increase in A_c (Colmenares *et al*. 2014, Hanna and Abdel-Rahman 1998, Huat *et al*. 2007, Mohamed and Austrell 2018). However, the Q_b increments are relatively large compared to the A_c increments, particularly at Site A. In addition, the Q_b increments evaluated by SLTs at the base settlement of 40 mm at Site B exceed the A_c increments. For Pile-I60, the Q_b increments are in the range of 50.8–126.8%, which generally exceeds the corresponding A_c increment of 53.3%. Therefore, Fig. 10 suggests that the use of an inclined base plate exerts an additional effect on Q_b over and above the observed A_c increment.

4.1.3 Extended rupture surface

The unit bearing capacity (q_u) of a general shallow foundation is expressed as follows (Terzaghi 1943, Acharyya 2019):

$$q_u = c'N_c^* + qN_q^* + \gamma DN_\gamma^* \quad (1)$$

where c′ and γ are the cohesion and unit weight of soils, respectively, and D is the width of the foundation. q depicts the overburden pressure on the foundation, which is equal to γL, where L represents the length of the foundation. N_c^*, N_q^*, and N_γ^* are bearing capacity factors, which depend on the foundation type and soil conditions. A relation for evaluating the end bearing capacity of the embedded pile can be deduced using Eq. (1), because the behavior at the base of an embedded pile is similar to that of shallow foundations. Note that the value of γDN_γ^* is significantly lower than that of qN_q^* because pile diameters (D) are relatively small compared to pile lengths (L). Thus, Eq. (1) can be reduced as follows:

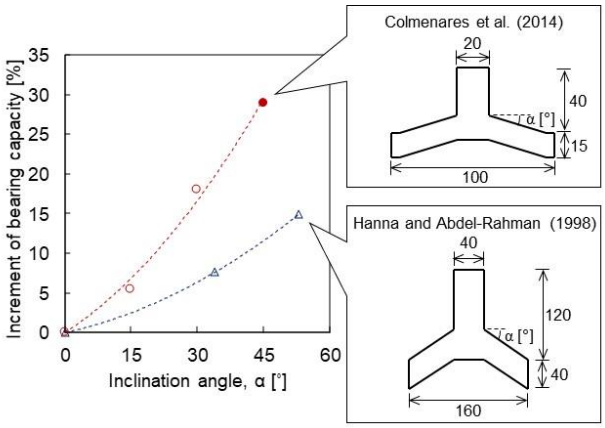

Fig. 11 Bearing capacity increments with respect to inclination angle of shell foundation (All dimensions are given in mm. Open circles and triangles depict experimental results, and a solid circle represent the theoretical result)

$$q_b = c'N_c^* + q'N_q^* \quad (2)$$

where q_b is the unit end bearing capacity of a pile foundation, and q′ denotes the effective vertical stress at the pile base. The projected area is used for the estimation of the end bearing capacity as follows:

$$Q_b = A_p q_b = A_p(c'N_c^* + q'N_q^*) \quad (3)$$

where Q_b and A_p are the end bearing capacity and projected area of the pile, respectively. For the evaluation of Q_b, Meyerhof (1976) suggested a relationship between the friction angle of soils (ϕ′) and N_q^* obtained from field tests conducted on pile foundations driven in sands. Vesic (1963), in contrast, derived a relationship between ϕ′ and N_c^* or N_q^* using the cavity expansion theory. Furthermore, Berezantzev *et al*. (1961) and Norlund (1963) proposed bearing capacity factors based on laboratory and field test results, whereas Janbu (1976) determined bearing capacity factors as functions of ϕ′ using numerical analyses.

Changing the foundation shape has been applied as a method to increase the bearing capacity of shallow foundations, particularly shell foundations. Shell foundations are shallow foundations, that adopt the shell shape to enhance the bearing capacity (Kurian and Devaki 2005). The shell foundations are commonly shaped as funnels, as depicted in Fig, 11, and previous studies have demonstrated that the bearing capacity of shell foundations is higher than that of flat shallow foundations (Colmenares *et al*. 2014, Hanna and Abdel-Rahman 1990, Kurian and Devaki 2005). Hanna and Abdel-Rahman (1990) and Colmenares *et al*. (2014) investigated trends in the bearing capacity of shell foundations with respect to the inclination angle (α), as described in Fig. 11. By installing model shell foundations in a chamber and subsequently conducting load tests, the bearing capacities were evaluated, and rupture surfaces were observed. Further, Hanna and Abdel-Rahman (1990) and Colmenares *et al*. (2014) suggested bearing capacity formulations and factors based on their observations of the rupture surface and increments in the bearing capacity with increasing α (Fig. 11). The increase in the bearing capacity was quantified in terms of the size of the rupture surface below the foundation. The rupture surface becomes larger and deeper as α increases (Colmenares *et al*. 2014, Hanna and Abdel-Rahman 1990). In addition, Han *et al*. (2020) observed that the shear wave velocity below the pile base increases as the inclination angle of the base plate increases. The higher shear wave velocity, which indicates the greater horizontal effective stress, may lead to a higher base resistance. The greater horizontal effective stress corresponds to a larger rupture surface.

The base shapes of Pile-Is considered in this study are similar to those of the shell foundations presented in Fig. 11. Further, the behavior at the base of an embedded pile is almost identical to that of shallow foundations, rather than driven pile, as the skin friction of embedded piles is achieved by a cement paste, which is weaker than the PHC pile. Thus, Q_b is analyzed theoretically in terms of α using the results obtained by Hanna and Abdel-Rahman (1990) because the rupture surfaces of the embedded pile cannot be observed in the field tests in this study. The relationship between N_q^* and α may be expressed as follows (Hanna and Abdel-Rahman 1990):

$$N_q^* = exp[\pi \cdot tan(\phi' + 2\beta)] \cdot tan^2(\frac{\pi}{4} + \frac{\phi'}{2} + \beta) \quad (4)$$

where β is an experimentally determined parameter associated with α as follows (Hanna and Abdel-Rahman 1990):

$$\beta = \frac{1}{60}\alpha \quad (5)$$

Note that the units of α and β are given in degrees. Because the cohesion of sands is negligible (c′ = 0), Eq. (3) is reduced as follows:

$$Q_b = A_p q' N_q^* \quad (6)$$

The end bearing capacity (Q_b) of a pile embedded in sands is proportional to the projected pile base area (A_p) and bearing capacity factor (N_q^*), as described in Eq. (6). Note that the projected areas (A_p) of Pile-C and Pile-Is are 1963.5 cm^2 and 2463.0 cm^2, respectively. If the measure of the rupture surface (S_r) is defined to be the product of the projected area and the bearing capacity factor, as described

in Eq. (7), Eq. (6) can be expressed as Eq. (8).

$$S_r = A_p N_q^* \tag{7}$$

$$Q_b = S_r q' \tag{8}$$

Assuming ϕ' to be 40°, N_q^* corresponding to α of 0°, 30°, 45°, and 60° are calculated, and the results are summarized in Table 6. N_q^* of Pile-I30, I45, and I60 exhibit increases of 15.1%, 23.7%, and 33.0%, respectively, compared to that of Pile-C. As observed in Eqs. (6) and (8), Q_b is proportional to S_r, which is the product of A_p and N_q^*. Consequently, theoretical Q_b increments of Pile-I30, I45, and I60 are 44.4%, 55.1%, and 66.8%, respectively. Moreover, theoretical Q_b increments with friction angles (ϕ') of 30°, 35°, 40°, 45°, and 50° are calculated and plotted in Fig. 12. Fig. 12 indicates that the theoretical Q_b increment increases with an increase in the inclination angle for a given friction angle. Note that Eq. (4) was obtained from model tests performed on shell foundations. The size of inclined parts for the shell foundations, as shown in Fig. 11, is larger than those for the Pile-Is, as shown in Fig. 3. Thus, the shape of the shell foundation changes more significantly than that of Pile-Is as the inclination angle (α) increases. The rupture surface below the shell foundation may likewise change more significantly than that below Pile-Is.

4.1.4 Quantitative factors affecting end bearing capacity

Experimental and analytical Q_b increments (because of the increased projected area, contact area, and rupture surface) are plotted with respect to the inclination angle (α) of the base plate in Fig. 13, which demonstrates that Q_b increases with an increase in α, although variations in Q_b exists. Fig. 13 shows that because the projected areas (A_p) of Pile-Is are the same, the A_p increments of all Pile-Is are identical. Moreover, because the contact area (A_c) of Pile-Is increases in a parabolic shape, the A_c increment increases with an increase in the inclination angle (α). Meanwhile, the increment in rupture surface (S_r), which is obtained from the bearing capacity factors and projected areas, is larger than those of A_p and A_c for all α and increases linearly with respect to α. Note that the S_r in Fig. 13 are obtained at a friction angle of 40°.

The experimental Q_b increments represented in Fig. 13 are selected at the relatively large settlement (max. s, s = 40 mm, and s = 10% of the pile diameter) for the comparison of the (ultimate) end bearing capacity, instead of the baseresistance, at each settlement. Therefore, the experimental Q_b increments may be compared to the analytical Q_b increments. Fig. 13 shows that the Q_b increment with respect to the rupture surface (S_r) is in relatively good agreement the experimental Q_b increment compared with the Q_b increment in terms of the projected area (A_p) and the contact area (A_c). In addition, the average Q_b increments at the relatively large base settlements (max. s or s = 40 mm), which are 36.5, 50.5, and 67.8% for Pile-I30, I45, and I60, respectively, are comparable to the Q_b increments at the base settlement of s = 10% of the pile diameter obtained from the laboratory test (Han *et al*. 2020)

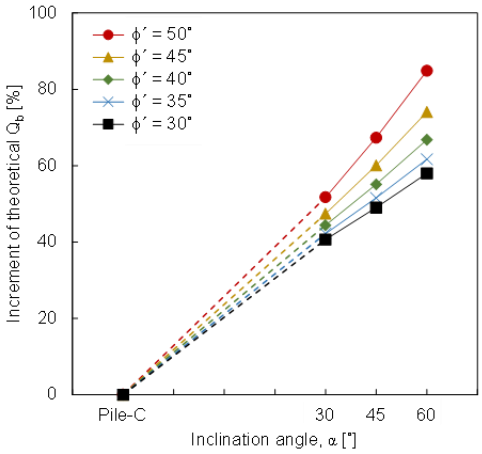

Fig. 12 Theoretical increments of end bearing capacity ($Q_b=S_rq'=A_pN_q^*q'$) with respect to inclination angle of base plate

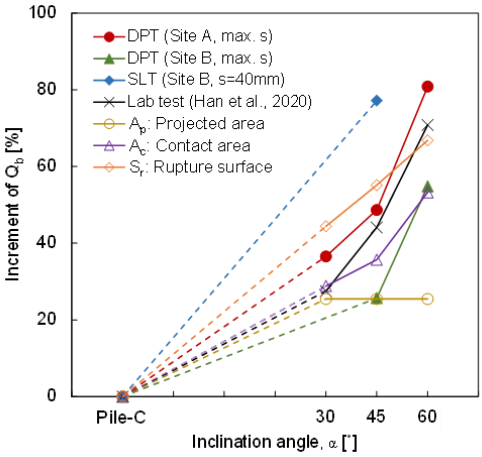

Fig. 13 Q_b increments determined by experiments and analyses with respect to inclination angle of base plate. (S_r is calculated with the assumption of a friction angle of 40°. Note that Q_b obtained by the laboratory test refers to the base resistance at the base settlement of 10% of the pile diameter)

as summarized in Table 3. However, for the field test results, some of the experimental Q_b increments are greater than the theoretical Q_b increments as presented in Fig. 13. Therefore, the use of inclined base plates may result in additional effects on Q_b, over those of quantitative factors, such as increased A_p, A_c, and S_r.

4.2 Qualitative factor – Enhanced slime discharge

Piles with inclined base plates may offer several advantages in terms of construction. Enhancement of slime discharge is a factor responsible for the increase in Q_b by improving the construction quality. The installation of embedded piles or drilled shafts requires the ground to be bored below the water tables. Thus, disturbed soils produced during excavations, tend to mix with water, and form a loose slurry that is commonly known as slime. Slime deteriorates the bearing capacity of embedded piles and

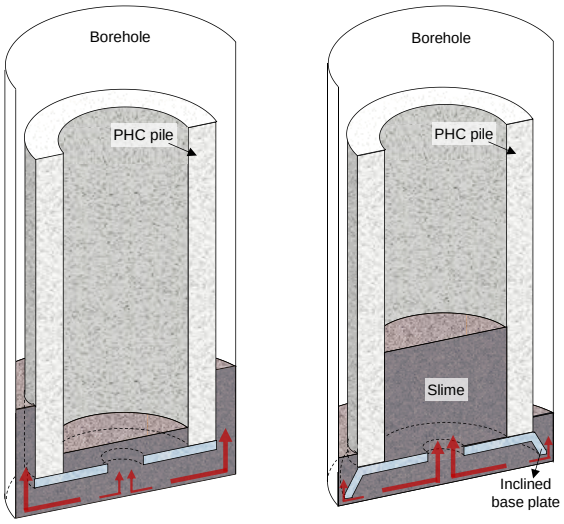

(a) Pile-C (b) Pile-I60

Fig. 14 Comparison of slime discharge according to the base shape (Red arrows mean the direction of slime flow)

drilled shafts (Ho 2003, Massarsch *et al*. 1988, Mullins *et al*. 2006, Neely 1991, Seo *et al*. 2003, Roscoe 1983, Shrivastava *et al*. 2016). The skin friction of the embedded piles is especially controlled by the strength of the cement paste injected into the space between the borehole and pile (Park *et al*. 2017). Disturbed soils and slime weaken the strength of the cement paste, thereby resulting in reduced skin friction (Paik 1997). Slime, which accumulates below the pile base, may also lead to increased settlement and reduced end bearing capacity. Thus, slime should be appropriately treated (Camp *et al*. 2002, Seo *et al*. 2003).

Bases of Pile-Is are shaped in the form of a funnel as depicted in Fig. 3. For the comparison of slime discharge at pile bases, conceptual schematics of Pile-C and I60 are presented in Figs. 14(a) and 14(b), respectively. As the projected area of Pile-I60 is larger than that of Pile-C, the gap between the bore hole and pile is smaller. Thus, the amount of slime that passes through the gap is less. Secondly, the inclined base plate tends to gather the slime, and discharge the slime through the pile hole. Therefore, relatively less slime remains under Pile-I60 (Fig. 14(b)) compared to that under Pile-C (Fig. 14(a)). With significant amounts of slime remaining near the base of Pile-C, the cement paste may not be sufficiently cured, and the end bearing capacity and skin friction of the lower part of the pile decrease. Thus, the increase in the end bearing capacity of Pile-Is compared to Pile-C may be attributed to the enhanced slime discharge caused by the inclined base plates.

5. Conclusions

In this study, seven test piles were installed in two fields to investigate the effects of incorporating inclined base plates on the end bearing capacity of embedded piles. The diameter of test piles is 50 cm, and the lengths of piles are 12 m at Site A and 14 m at Site B, respectively. A conventional PHC pile (Pile-C) and piles with enlarged base plates inclined at 30°, 45°, and 60° (Pile-I30, I45, and I60, respectively) were installed at Site A, whereas Pile-C, I45, and I60 were installed at Site B. All test piles were installed using the embedded pile method. The diameter of the inclined base plates is 56 cm, and the projected area of Pile-Is is 2463.0 cm^2, which is larger by 25.4% than that of Pile-C at 1963.5 cm^2. The standard penetration resistances, SPT N-values, near pile bases at Sites A and B are 50/6–50/2 and 50/8–50/4, respectively. To investigate the base resistance of test piles, dynamic pile tests were conducted during pile construction at Sites A and B according to ASTM D4945. Furthermore, static load tests were conducted according to ASTM D1143 after curing the cement paste. The load – settlement curves at the pile bases were obtained from dynamic pile tests and static load tests. The base resistances of piles with different base shapes were experimentally analyzed with respect to the inclination angle of the base plate. The increase in the base resistance was quantitatively and qualitatively analyzed in terms of the increased projected area, increased contact area, extended rupture surface, and enhanced slime discharge.

Field tests indicate that the base resistances of Pile-Is are larger than those of Pile-C. Further, the base resistances of Pile-Is increase with an increase in the inclination angle of the base plate. An increase in the projected area (closed-ended cross-sectional area of the PHC pile) of Pile-Is leads to an enhanced base resistance. The unit base resistance in Pile-Is increases typically with an increase in the inclination angle. In addition, the contact area between the pile base and soils likewise influences the effect of inclined base plates on the base resistance. As the inclination angle of Pile-Is increases, the contact area increases, leading to an increase in the base resistance. Larger inclination angles cause larger and deeper rupture surfaces, which indicate the greater bearing capacity factor. In addition to the quantitative factors such as the projected area, contact area, and rupture surface, the qualitative factor such as slime discharge is considered. Slime discharge is an important factor in the construction of embedded piles. Piles with inclined base plates may effectively discharge slime under the inclined base plate through the pile hole. Thus, the base resistance increases with an increase in the inclination angle. This study demonstrates that the optimum design of an embedded pile with respect to the end bearing capacity may be achieved using the inclined base plates.

Acknowledgments

This work was supported by the Korean Small Business Innovation Research Program grant funded by the Korea Land & Housing Corporation and the National Research Foundation of Korea (NRF) grant funded by the Korea government (MSIT) (No. NRF-2021R1A5A1032433).

References

Acharyya, R. (2019), "Finite element investigation and ANN-based prediction of the bearing capacity of strip footings resting on sloping ground", *Int. J. Geo-Eng.*, **10**, 5.

https://doi.org/10.1186/s40703-019-0100-z.
ASTM D1143 (2013), Standard test methods for deep foundations under static axial compressive load, ASTM International, West Conshohocken, Pennsylvania, U.S.A.
ASTM D4945 (2008), Standard test methods for high-strain dynamic testing of deep foundations, ASTM International, West Conshohocken, Pennsylvania, U.S.A.
Berezantzev, B., Khrisoforov, V. and Golubkov, V. (1961), "Load bearing capacity and deformation of piled foundations", *Proceedings of the 5th International Conference on Soil Mechanics and Foundation Engineering*, Paris, France, July.
Camp, W.M., Brown, D.A. and Mayne, P.W. (2002), "Construction method effects on axial drilled shaft performance", *Proceedings of the Deep Foundations 2002: An International Perspective on Theory, Design, Construction, and Performance*, Orlando, Florida, U.S.A., February.
Colmenares, J.E., Kang, S.R., Shin, Y.J. and Shin, J.H. (2014), "Ultimate bearing capacity of conical shell foundations", *Struct. Eng. Mech.*, **52**(3), 507-523. http://doi.org/10.12989/sem.2014.52.3.507.
Fellenius, B.H. (2002), "Determining the true distributions of load in instrumented piles", *Proceedings of the Deep Foundations 2002: An International Perspective on Theory, Design, Construction, and Performance*, Orlando, Florida, U.S.A., February.
Fellenius, B.H. and Terceros, M.H. (2014), "Response to load for four different bored piles", *Proceedings of the DFI/EFFC International Conference on Piling and Deep Foundations*, Stockholm, Sweden, May.
Han, K., Seo, M.J., Hong, W.T. and Lee, J.S. (2020), "End-bearing capacity of embedded piles with inclined-base plate: Laboratory model tests", *J. Geotech. Geoenviron. Eng.*, **146**(8), 04020063. https://doi.org/10.1061/(ASCE)GT.1943-5606.0002304.
Hanna, A. and Abdel-Rahman, M. (1990), "Ultimate bearing capacity of triangular shell strip footings on sand", *J. Geotech. Eng.*, **116**(12), 1851-1863. https://doi.org/10.1061/(ASCE)0733-9410(1990)116:12(1851).
Hanna, A. and Abdel-Rahman, M. (1998), "Experimental investigation of shell foundations on dry sand", *Can. Geotech. J.*, **35**(5), 847-857. https://doi.org/10.1139/t98-049.
Ho, C.E. (2003), "Base grouted bored pile on weak granite", *Proceedings of the Third International Conference on Grouting and Ground Treatment*, New Orleans, Louisiana, U.S.A., February.
Hong, H.S., Cho, C.W., Lee, M.W. and Lee, W.J. (1997), "Failure of precast piles installed by preboring method and the remedial measures", *Proceedings of the International Conference on Foundation Failures*, Singapore, August.
Hong, W.P. and Chai, S.G. (2003), "The skin friction capacity of SDA (separated doughnut auger) pile", *Proceedings of the Thirteenth International Offshore and Polar Engineering Conference*, Honolulu, Hawaii, U.S.A., May.
Huat, B.B.K., Mohammed, T.A., Abang Ali, A.A.A. and Abdullah, A.A. (2007), "Numerical and field study on triangular shell footing for low rise building", *Int. J. Eng. Technol.*, **4**(2), 194-204.
Janbu, N. (1976), "Static bearing capacity of friction piles", *Sechste Europaeische Konferenz fuer Bodenmechanik und Grundbau*, **1**(3), 1-26.
Karkee, M.B. (1999), "Developments in low noise and low vibration methods of pile installation in Japan", *Proceedings of the 11th Asian Regional Conference on Soil Mechanics and Geotechnical Engineering*, Seoul, Korea, August.
Kurian, N.P. and Devaki, J.V.M. (2005), "Analytical studies on the geotechnical performance of shell foundations", *Can. Geotech. J.*, **42**(2), 562-573. https://doi.org/10.1139/t04-110.
Massarsch, K.R., Brieke, W. and Tancre, E. (1988), "Displacement auger piles with compacted base", *Proceedings of the International Geotechnical Seminar on Deep Foundations on Bored and Auger Piles*, Ghent, Belgium, June.
Meyerhof, G.G. (1976), "Bearing capacity and settlement of pile foundations", *J. Geotech. Eng. Div.*, **102**(GT3), 197-228.
Mohammed, W. and Austrell, P.E. (2018), "A comparative study of three onshore wind turbine foundation solutions", *Comput. Geotech.*, **94**(1), 46-57. https://doi.org/10.1016/j.compgeo.2017.08.022.
Mullins, G., Winters, D. and Dapp, S. (2006), "Predicting end bearing capacity of post-grouted drilled shaft in cohesionless soils", *J. Geotech. Geoenviron. Eng.*, **132**(4), 478-487. https://doi.org/10.1061/(ASCE)1090-0241(2006)132:4(478).
Neely, W.J. (1991), "Bearing capacity of auger-cast piles in sand", *J. Geotech. Eng.*, **117**(2), 331-345. https://doi.org/10.1061/(ASCE)0733-9410(1991)117:2(331).
Norlund, R.L. (1963), "Bearing capacity of piles in cohesionless soils", *J. Soil Mech. Found. Div.*, **89**(3), 1-36.
Paik, K.H. (1997), "Characteristics of the bearing capacity for new auger-drilled piles", *J. Kor. Geotech. Soc.*, **13**(4), 25-35.
Park, J.J., Jung, G.J. and Jeong, S.S. (2017), "The analysis of skin friction on small-scale prebored and precast piles considering cement milk influence", *J. Kor. Geotech. Soc.*, **33**(1), 5-15. https://doi.org/10.7843/kgs.2017.33.1.5.
Pile Dynamics Inc. (2014), "CAPWAP background report Version 2014", Pile Dynamics Inc., Cleveland, Ohio, U.S.A.
Roscoe, G.H. (1983), "The behavior of flight auger bored piles in sand", *Proceedings of the International Conference on Advances in Piling and Ground* Treatment, London, U.K., March.
Seo, Y.H., Cho, S.H., Choi, D.W. and Han, B.K. (2003), "A study on the optimum design guide for auger-drilled piling", *J. Kor. Soc. Civ. Eng.*, **51**(7), 8-16.
Shrivastava, A.K., Jain, D. and Vishwakarma, S. (2016), "Frictional resistance of drilling fluids as a borehole stabilizers", *Int. J. Geo-Eng.*, **7**, 12. https://doi.org/10.1186/s40703-016-0026-7.
Terzaghi, K. (1943), *Theoretical Soil Mechanics*, Wiley, New York, U.S.A.
Vesic, A.B. (1963), *Bearing Capacity of Deep Foundations in Sand*, Highway Research Record, Washington, D.C., U.S.A.
Yoo, C.S., Kim, S.B., Heo, K.S. and Song, K.Y. (2007), "End bearing capacity of pile tip-enlarged PHC piles in weathered rock", *J. Kor. Geotech. Soc.*, **23**(1), 23-37.
Zou, J.F., Yang, T. and Deng, D. (2019), "Field test of the long-term settlement for the post-grouted pile in the deep-thick soft soil", *Geomech. Eng.*, **19**(2), 115-126. http://doi.org/10.12989/gae.2019.19.2.115.

GC